

## Synthesis, Characterization and Application of Lead Sulfide Nanostructures as Ammonia Gas Sensing Agent

Hassan Karami<sup>1,2,\*</sup>, Mina Ghasemi<sup>1</sup>, Sara Matini<sup>1</sup>

<sup>1</sup>Nano Research Laboratory, Department of Chemistry, Payame Noor University, Abhar, Iran

<sup>2</sup>Department of Chemistry, Payame Noor University, 19395-4697, Tehran, I.R. of Iran

\*E-mail: [karami\\_h@yahoo.com](mailto:karami_h@yahoo.com)

Received: 2 July 2013 / Accepted: 18 August 2013 / Published: 10 September 2013

---

In this paper, different lead sulfide nanostructures such as nanoparticles and nanowires are synthesized by chemical precipitation. To obtain a sample with uniform morphology and pure composition, we investigated and optimized the amounts of experimental variables such as sodium sulfide and lead acetate concentrations, types and concentration of synthesis additives, pH, bath temperatures, and ultrasonic wave irradiation. The prepared samples are characterized by SEM, TEM, EDX, XRD, TGA, DTA, and UV-visible spectroscopy. The optimized conditions include 0.5% lead acetate, 1% sodium sulfide, pH 3, 20 KHz ultrasonic irradiation with power of 2230 W cm<sup>-2</sup>, 25 °C solution temperature, and 0.5% wt sodium dodecyl sulfate as structural additive. In optimum conditions, uniform PbS nanowires with 40 nm average diameter and 5 μ average lengths are synthesized. The optimized PbS nanowires were used as an ammonia gas-sensing agent to construct a new solid-state sensor. This sensor showed high dynamic range and sensitivity to ammonia gas. The interference of NO<sub>2</sub> on ammonia response is decreased by adding ammonium chloride in sintering step.

---

**Keywords:** lead sulfide; nanowires; chemical synthesis; gas sensor; ammonia

### 1. INTRODUCTION

Semiconductor nanoparticles have good optical and electronic properties, and there has been much interest in the synthesis and characterization of sulfide nanoparticles [1-3]. Lead sulfide is an important IV-VI group semiconductor, which has attracted much attention because of its special small direct-band gap (0.41 eV) and large excitonic Bohr radius of 18 nm [4, 5].

Different morphologies can play roles in the properties. They include nanocrystals [6], nanorods [7, 8], nanotubes [7], nanocubes [9], star shapes [10], dendrites [9, 11], and flower-like crystals [12]. All can be prepared by different methods, such as hydrothermal and solvothermal [13, 9], vacuum deposition [14], electrochemical deposition [15], pulsed laser deposition [16], spray pyrolysis

[17], successive ionic layer adsorption reaction [18], photochemical [19], chemical bath deposition [20],  $\lambda$ -ray irradiation [21], sonochemical [6], and microwave radiation [7]. The lead sulfide nanoparticles have wide applications in many fields such as solar cells, solar absorbers, photographs, lasers, LED devices, telecommunications, detectors, optical switches, optical amplification, and also as gas-sensing agents in the solid-state sensors. Only a few reports about using PbS as a gas-sensing agent are available. Markov and Maskaeva reported some interesting data about using a PbS film as a solid-state sensor to detect nitrogen oxides, such as  $\text{NO}_2$  [22]. Fu reported a solid-state sensor based on lead sulfide to determine  $\text{NO}_2$  and  $\text{NH}_3$ . Recently, Bandyopadhyay synthesized nano-sized PbS based on the sol-gel method and showed that the synthesized nanocrystalline PbS was influenced predominantly by  $\text{NH}_3$  and  $\text{NO}_2$  amongst many other gases at room temperature [23]. In this work, we report a simple, repeatable, and controllable method to synthesize lead sulfide nanostructures (nanoparticles and nanowires) based on a rate-controlling precipitation. The effects of all synthesis parameters were optimized to obtain a uniform lead sulfide nanowire. An optimized lead sulfide sample was used to construct a solid-state sensor to detect the ammonia gas.

## 2. EXPERIMENTAL

### 2.1. Materials

Lead acetate  $\text{Pb}(\text{CH}_3\text{COO})_2$ , sodium sulfide ( $\text{Na}_2\text{S}$ ),  $\text{NaOH}$ , and  $\text{HNO}_3$  were purchased from Merck and polyvinyl pyrrolidone (PVP), glycerol, and sodium dodecyl sulfate (SDS) were purchased from Fluka and Aldrich. Double-distilled water was used in all experiments.

### 2.2. Instrumental

Ultrasonic irradiation was exerted by ultrasonic probe (20 MHz Scientz ultrasonic instrument, China). The morphologies of the samples were characterized by the scanning electron microscopy (SEM, Philips, XL-30, Netherlands). A transmission electron microscope (TEM, Zeiss EM900, 80 keV) was used to measure the size and shape of particles accurately. UV-Visible absorption spectra were measured using a double-beam spectrophotometer (Shimadzu 2550). A thermogravimetric analysis (TGA) and differential thermal analysis (DTA) were simultaneously performed using a thermogravimetric analyzer (TGA/DTA, Mettler Toledo) for thermal studies.

### 2.3. Procedures

#### 2.3.1. Synthesis procedures

PbS nanoparticles were synthesized through rate control by adding lead acetate solution into the sodium sulfide solution to precipitate lead sulfide. The pHs of the solutions were adjusted by adding  $\text{HNO}_3$  or  $\text{NaOH}$  solutions. In this method, the mixing (adding) rate of two precursor solutions

(lead acetate and sodium sulfide) is a limiting factor to control the morphology and the particle sizes of samples. The other parameters, such as lead acetate concentration, sodium sulfide concentration, temperature, pH, structural director additives, and ultrasonic irradiation can affect the morphology, particle sizes, and composition of the synthesized samples. The resulting precipitates after filtration were washed two times with double-distilled water, then with acetone, and were dried in an oven at 80°C for 30 min. To prevent them from oxidation, the sample dish deoxidized with N<sub>2</sub>. The synthesis conditions, including lead acetate concentration, sodium sulfide concentration, temperature, pH, structure director additives, and ultrasonic irradiation, were investigated and optimized by the “one-at-a-time” method to obtain a sample with the best size and morphology. The morphology and particle sizes of the lead sulfide nanopowders were characterized by SEM and TEM. XRD patterns (using Cu [K<sub>α</sub>] radiation with  $\lambda = 0.15418$  nm) were used to determine the composition of the samples.

### 2.3.2. Construction of gas-sensing device

A sensor device (microchip) was constructed by the copper electroless followed by gold electroplating. The gas-sensor device was 5 cm × 7 cm, including two gold comb electrodes with 0.2 mm interval distance. We dispersed 0.2 g PbS nanopowder (synthesized under optimum conditions) in 5 ml of acetone by ultrasonic shaking for 2 h to obtain a homogenous suspension. After completing homogenization, we painted the slurry on all surfaces of the sensor microchip. The painted microchip was kept in 80°C for 10 min, enabling the slurry to dry as a thin nanostructured film. The coated microchip was cured at different temperatures (110, 120, 130, 140, 150, 200, and 250 °C) for 3 h to determine a suitable cohesion temperature of the lead sulfide nanoparticles, enabling them to adhere to one another and to the microchip surface.

The cured chip was input into a glassy cubic box of 200 L total volume. A small electric fan was used to make fast homogenization of the gas mixture in the box. The different volumes of some gases, such as NH<sub>3</sub>, Air, CO, CO<sub>2</sub>, SO<sub>2</sub>, NO, and NO<sub>2</sub> were injected into the box, and the sensor resistance was measured.

## 3. RESULTS AND DISCUSSION

Lead sulfide nanoparticles were synthesized by the rate control of adding lead acetate solution to the sodium sulfide solution. In the present method, there are some parameters, such as the mixing rate of lead acetate with sodium sulfide solutions, lead acetate and sodium sulfide concentrations, pH, solution temperature, type and concentration of synthesis additive, and the power of ultrasonic irradiation, which these amounts optimized by the "one-at-a-time" method. The synthesized samples were characterized by the SEM, TEM, and X-ray diffraction, Energy dispersive X-ray spectroscopy (EDX), UV-Vis spectroscopy, and TGA and DTA analyses. In the chemical precipitation process, the mixing rate of two precursors (lead and sulfide ions) is an important parameter to control a synthesis product. An initial full investigation showed that the 5 ml min<sup>-1</sup> is suitable to prepare lead sulfide

nanostructures. The following sections of this paper describe the optimization experiments of the other parameters.

After optimization of synthesis conditions, the PbS nanowires were used as an ammonia gas-sensing agent to construct a new solid-state sensor. This sensor ability for measurement of the different gases, such as  $N_2$ , Air, CO,  $CO_2$ , NO,  $SO_2$ ,  $NO_2$ , and  $NH_3$ , was investigated, and the changes in the sensor resistance versus gas concentration along with its response time to different gases, were studied to recognize an appropriate gas with the highest sensitivity, widest linear range, and shortest response time. Among the cited gases, the constructed sensor showed a high dynamic range, high sensitivity, and short response time to ammonia. The interference of  $NO_2$  on the sensor response to ammonia was decreased by adding ammonium chloride to the lead sulfide slurry before the curing step.

### 3.1. Optimization of lead acetate concentration

In the second step (after optimization of the mixing rate), the effects of lead acetate concentration were investigated on the morphology and particle sizes of the synthesized PbS samples. The lead acetate concentration was varied from 0.25% to 3% wt, and the other parameters were kept constant (1% wt sodium sulfide, a pH of 5 for lead acetate solution, a pH of 12 for sodium sulfide, and a temperature of  $25^\circ C$  without an additive or ultrasonic irradiation). The obtained samples were studied by SEM images (Fig. 1). Lead acetate is an initial reagent to produce PbS, and the reaction kinetic follows lead acetate concentration.

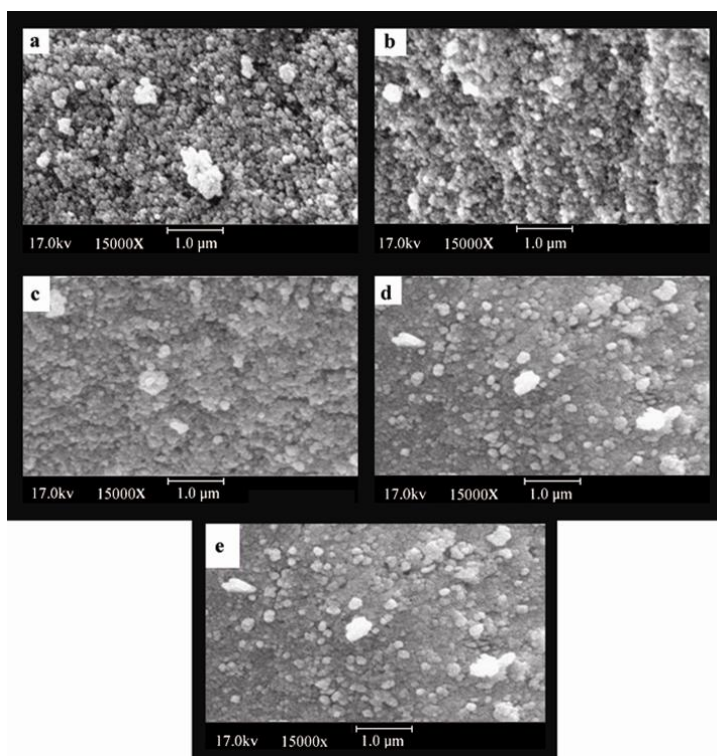


**Figure 1.** SEM images of the lead sulfide samples synthesized at different concentrations of lead acetate; 0.25 % (a), 0.5% (b), 1% (c), 2% (d), and 3% (e).

As we can see in Fig. 1, any increase in lead acetate concentration causes a speed-up formation of PbS nanoparticles [20] in the development of average particle sizes and also their agglomeration. Therefore the sample morphology turns into an undesirable form. This is probably due to the local supersaturation in the falling position of lead acetate solution drops. Thus the lead acetate concentration of 0.5% wt makes more uniform nanoparticles with average particle size 50 nm and with the best porosity; so the 0.5% wt was selected as the optimum concentration for further studies.

### 3.2. Optimization of sodium sulfide concentration

To investigate the effects of sodium sulfide concentration on the morphology and particle sizes of the synthesized PbS nanopowders, we varied the amount of this parameter from 0.5 % wt to 3 % wt while the amounts of the other parameters were kept constant. Figure 2 shows the SEM images of PbS samples that synthesized at different sodium sulfide concentrations. The role of sodium sulfide in the formation of PbS particles is similar with its lead acetate. The SEM images indicate that 1% wt of sodium sulfide concentration makes uniform nanoparticles with 80 nm average particle size. Therefore 1% can be used as a suitable amount to synthesize uniform nanoparticles.

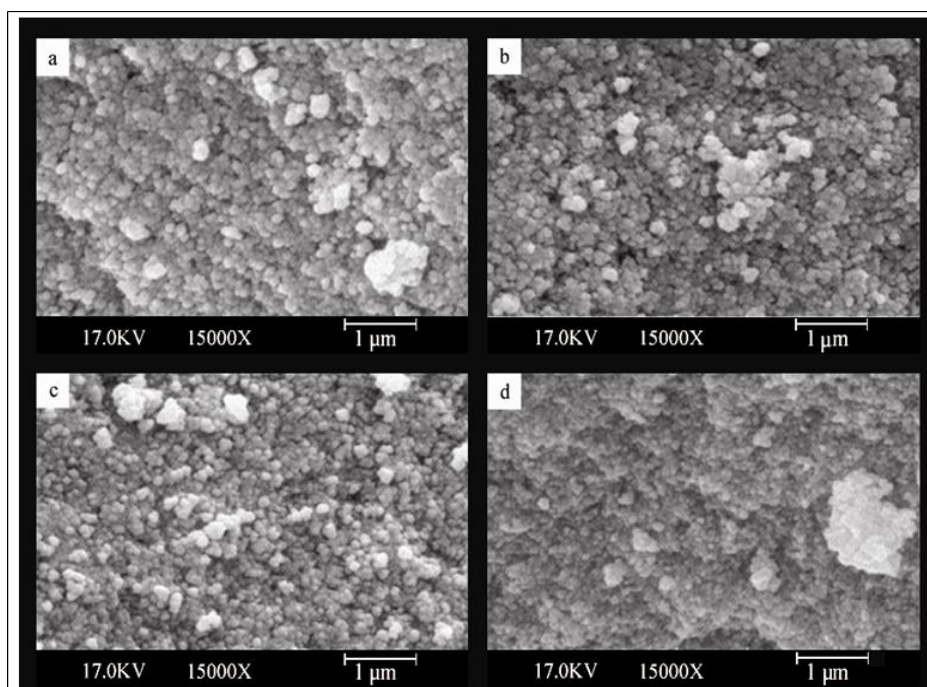


**Figure 2.** SEM images of the lead sulfide samples synthesized at different concentrations of sodium sulfide; 0.5% (a), 1% (b), 2% (c), 3% (d).

### 3.3. Effect of pH solution

The effect of pH solution was investigated on the morphology and particle sizes of the PbS samples. For this purpose, four samples were synthesized at pHs of 1, 2, 3, and 4 by adding HNO<sub>3</sub>. Figure 3 shows SEM images of the synthesized samples.

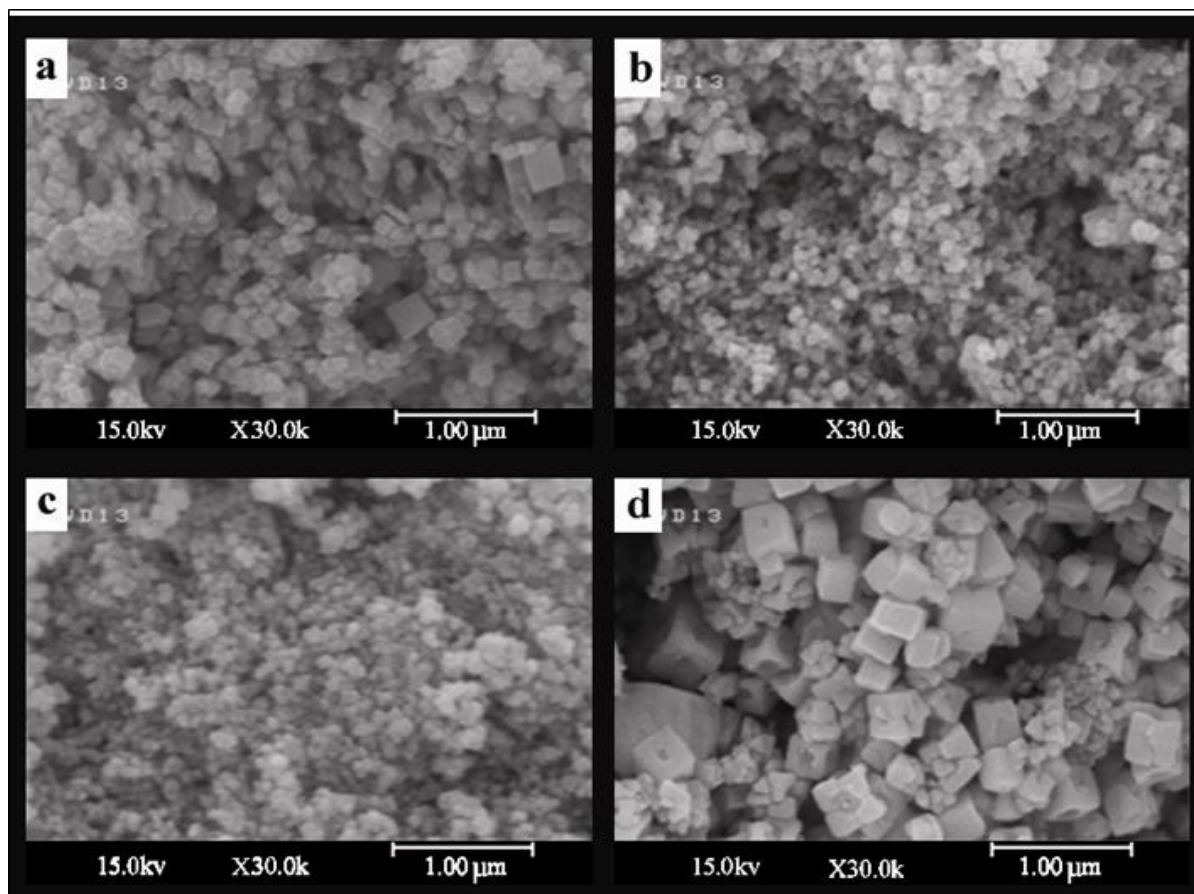


**Figure 3.** SEM images of the samples with different pHs; (a) 1, (b) 2, (c) 3, and (d) 4.

PbS nanoparticles have more uniform morphology in a pH of 2 and 3 than of 1 and 4. An increase in the average particle size in pH 4 perhaps is due to the formation of  $\text{Pb}(\text{OH})_2$ . There is another reason for an increase in particle size at pH 4. By increasing pH from 3 to 4, the free sulfide concentration is increased about 1000 times. Obviously,  $\text{H}_2\text{S}$  is a weak acid, and the molecular  $\text{H}_2\text{S}$  is the major form in lower pHs. The rate of PbS formation is controlled via slow dissociation of  $\text{H}_2\text{S}$  during the addition of lead acetate. Therefore in lower pHs, the rate of precipitation forming is slow; consequently the PbS particles have enough time to grow [19]. The average particle size is 90 nm in pH of 3, and that is smaller than in pH 2. Based on the obtained results, the pH solution of 3 is suitable to synthesize uniform PbS nanoparticles.

#### 3.4. Optimization of ultrasonic irradiation

In this step, the effects were investigated on the particle sizes, and the morphology of PbS samples was investigated. So we applied different powers of the ultrasonic irradiations 0, 956, 1593, 2230, and 2867  $\text{W cm}^{-2}$  (with respect to the surface area of the tip). The SEM images of the synthesized PbS samples by applying different powers of ultrasonic irradiation are seen in Fig. 4.

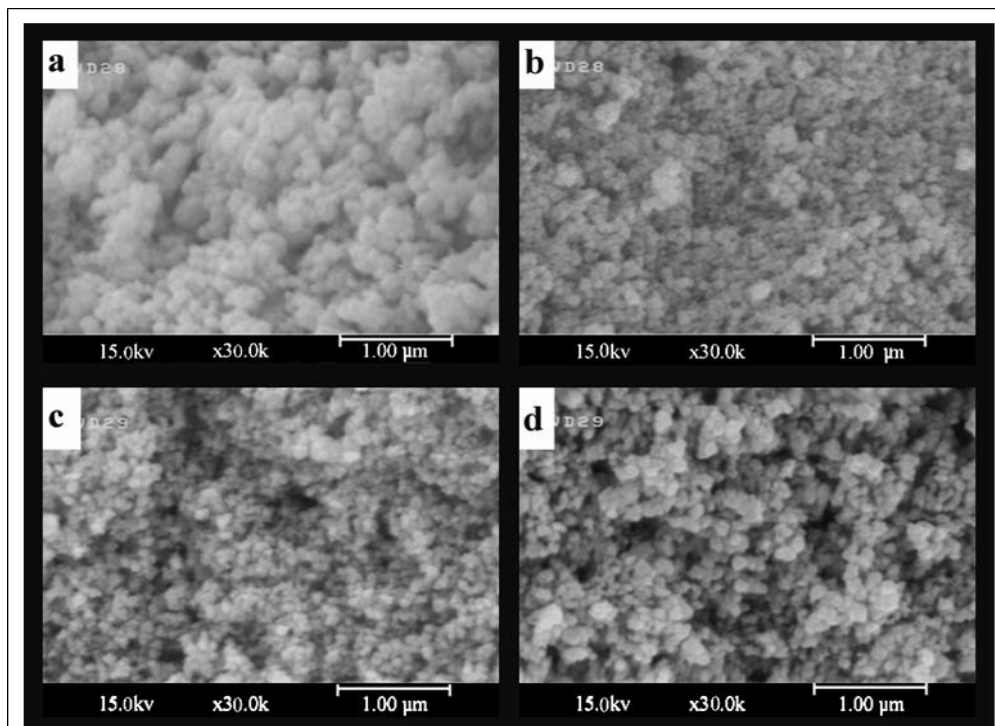


**Figure 4.** SEM images of the samples with different powers of ultrasonic wave radiation; (a) 30%, (b) 50%, (c) 70%, (d) 90%.

Because these SEM images show that by increasing the ultrasonic irradiation power from 0 to  $2230 \text{ W cm}^{-2}$ , the sizes of the particles are decreased because of mechanical abrasion. At higher ultrasonic powers, it is expected that hydroxyl radicals will be produced in the solution [24, 25]. The presence of hydroxyl radicals during the mixing of the reagents probably causes a change in the mechanism and consequently in the kinetics of PbS formation. Therefore the larger and agglomerated particles are seen in the higher ultrasonic powers. By using the  $2230 \text{ W cm}^{-2}$  ultrasonic irradiation, the 91 nm average particle diameters can be achieved.

### 3.5. Effect of synthesis temperature

To study the effects of temperatures, four samples were synthesized at different temperatures while amounts of the other parameters were kept constant. The prepared samples were characterized by SEM. Figure 5 shows SEM images of the PbS samples, which synthesized at 25, 50, 75, and  $90^\circ\text{C}$ . As the SEM images show, in this method the temperature has no sizable influence on either the particle sizes or the morphology of the PbS samples. For further study, the samples were analyzed by XRD. Figure 6 shows the XRD patterns of these samples at different temperatures. As seen in this figure, there are nine peaks in the XRD pattern related to each sample that are characteristic of PbS compound [26]. Also, the base peak height differs in various temperatures. To determine the particle sizes of the samples, we employed a Debye-Scherrer equation that is given by Eq. 1:

$$\text{(Eq. 1)} \quad D = \frac{0.9\lambda}{B \cos \theta}$$

Where,  $D$  (nm),  $\lambda$  (nm),  $\theta$  (degrees), and  $B$  (nm) are the average particle size, the X-ray wavelength, the diffraction angle and the maximum peak width in half-height, respectively. Table 1 shows the particle sizes at different temperatures based on XRD results and calculations from the Debye-Scherrer equation. The presented data show that the sample that synthesized at 25 °C has smaller particles with an average size of 92.3 nm.

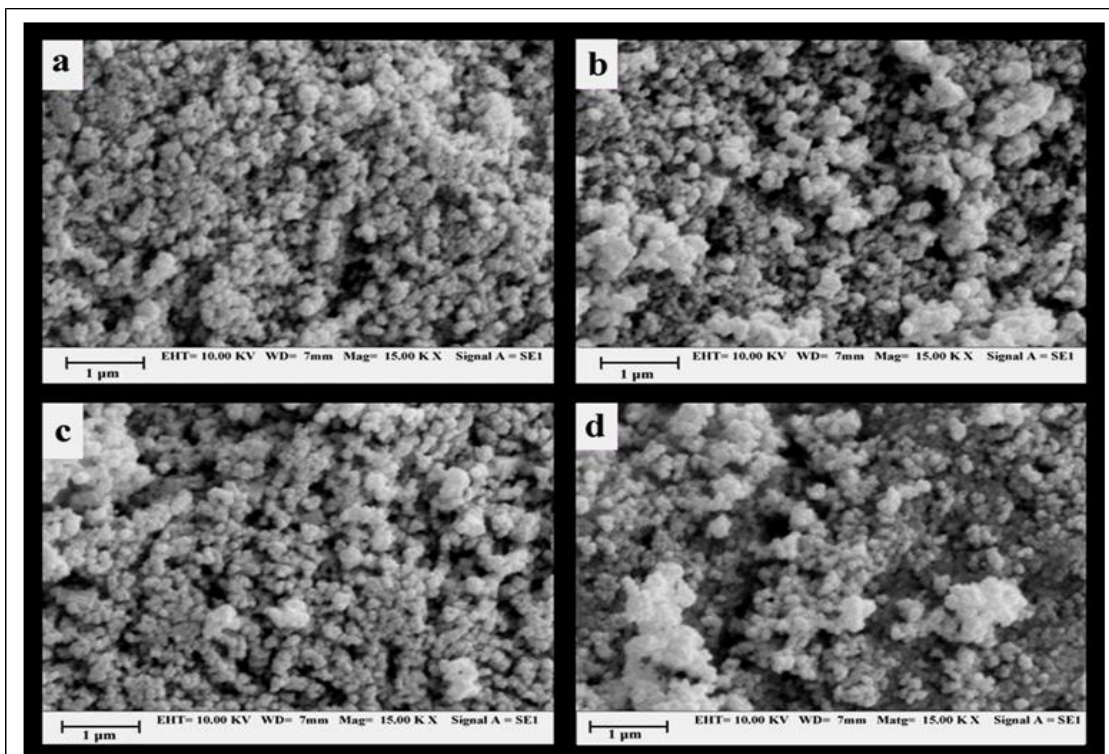


**Figure 5.** SEM images of the samples synthesized at different temperatures; (a) 25 °C, (b) 50 °C, (c) 75 °C, (d) 90 °C.

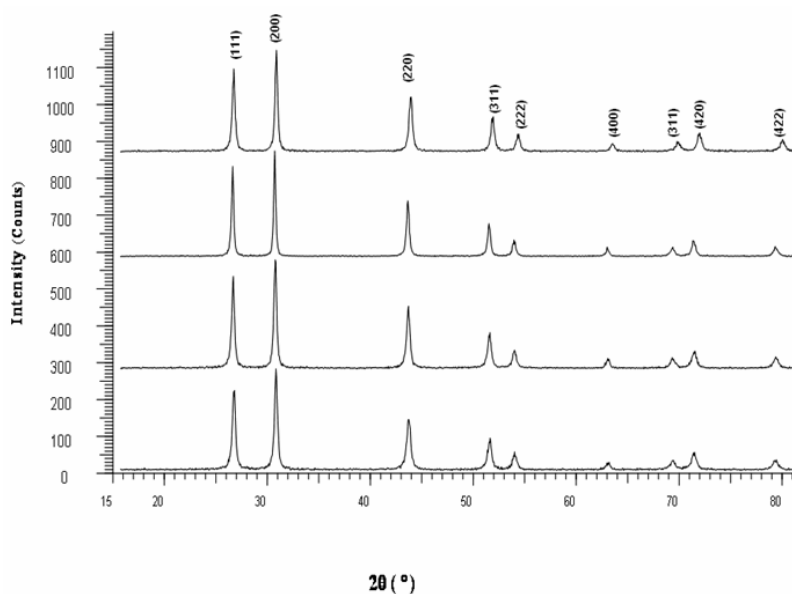


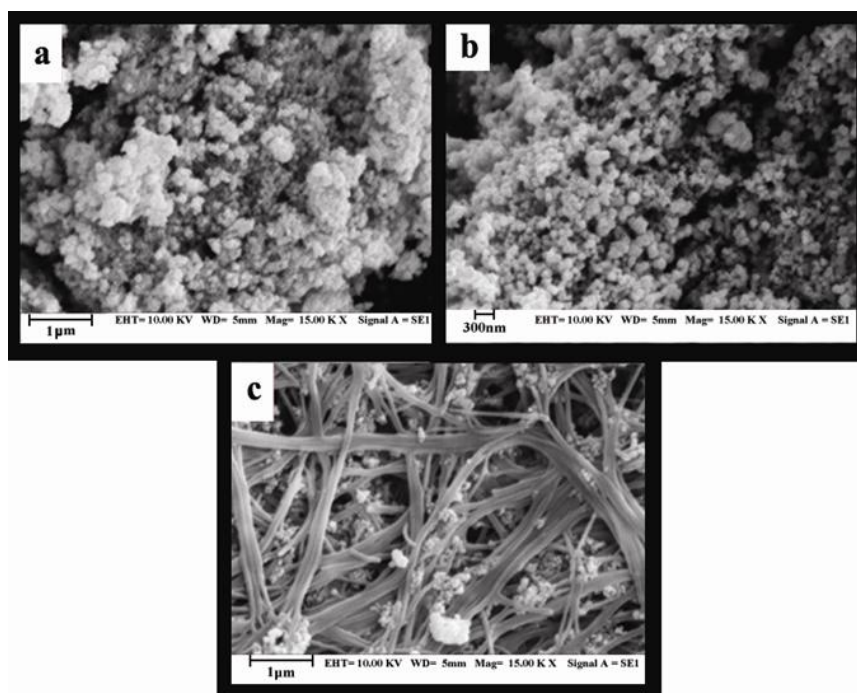
**Figure 6.** XRD patterns of the PbS samples synthesized at different temperatures; (a) 25 °C, (b) 50 °C, (c) 75 °C, (d) 90 °C.

**Table 1.** Variation of particles sizes versus synthesis temperatures

Temperature (°C)	Particle size (nm)
25	32
50	37
75	51
90	41

### 3.6. Effect of additive type

Surfactants are used as improving agents in nanomaterials synthesizes to control the mechanism and kinetics of the reaction. These additives can affect the morphology and particle sizes of the final product [27]. The size distribution of the nanoparticles can be controlled by adding a surfactant [28]. Different surfactants have been employed in the synthesizing of nanoparticles, such as sodium dodecyl sulfate (SDS), polyvinyl pyrrolidone (PVP), glycerol, bis(2-ethylhexyl) sulfosuccinate (AOT), cetyltrimethyl ammonium bromide (CTAB), and diethyl sulfosuccinate (DES) [29-31]. Among the synthesis parameters, the additive type had more effects on morphology of the synthesized PbS samples. In this study, the effects of PVP, SDS, and glycerol were investigated on the morphology and particle sizes of PbS nanoparticles, and the amounts of the other parameters of synthesis were kept constant. In the presence of PVP and glycerol, no change was noticed on the structure of the synthesized sample, but the results showed that SDS is more efficient in obtaining suitable morphology and more-uniform PbS nanowires (Fig. 7).

**Figure 7.** SEM images of the synthesized samples with different additive types; PVP (a), Glycerol (b), SDS (c).

Obviously, nanowires have high surface area in comparison with nanoparticles, and because of the semiconductor property of PbS, they have wide applications in electronic industries. Indeed, dodecyl sulfate anion forms a more stable complex compound with  $\text{Pb}^{2+}$  than two other surfactants. After the selection of SDS as a suitable additive, further study was performed to choose an optimum concentration for it. Figure 8 shows the effects of different concentrations of SDS on the morphology and particles sizes of PbS. As we see in Fig. 8, uniform PbS nanowires with minimum impurity can be obtained at 0.5% wt SDS.

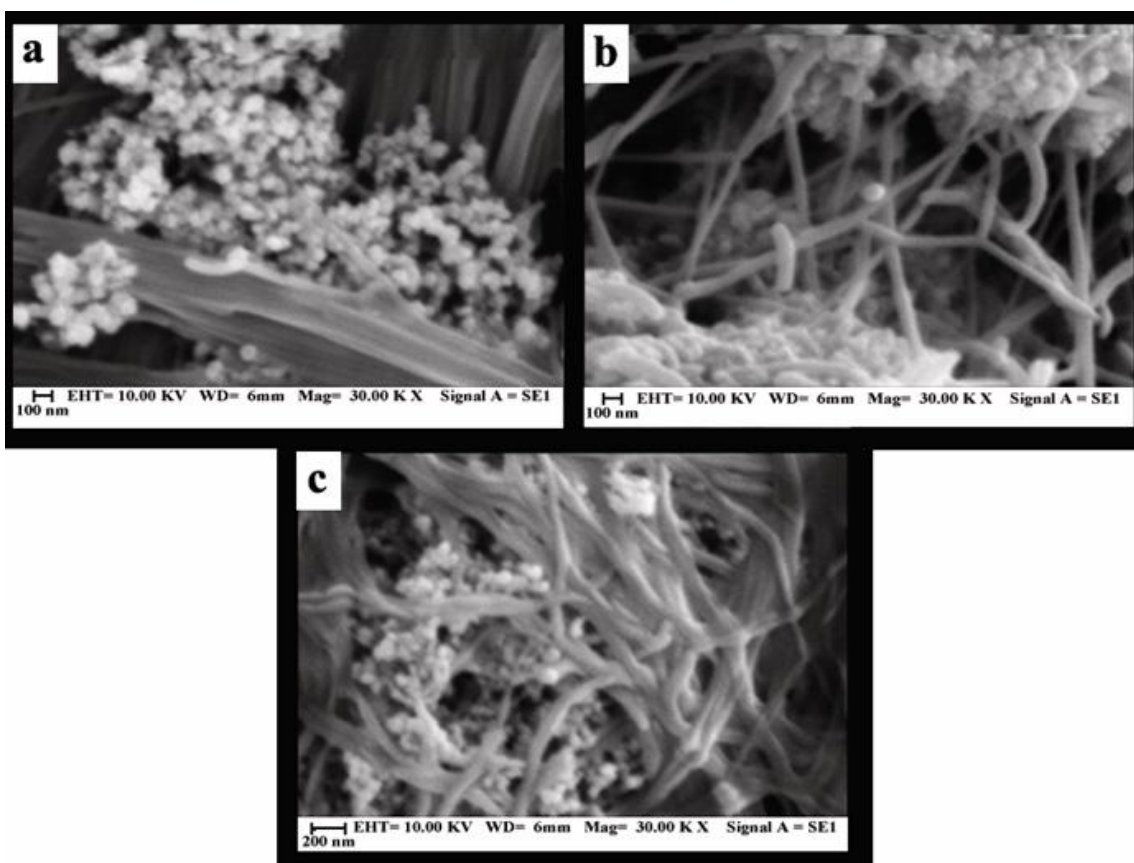
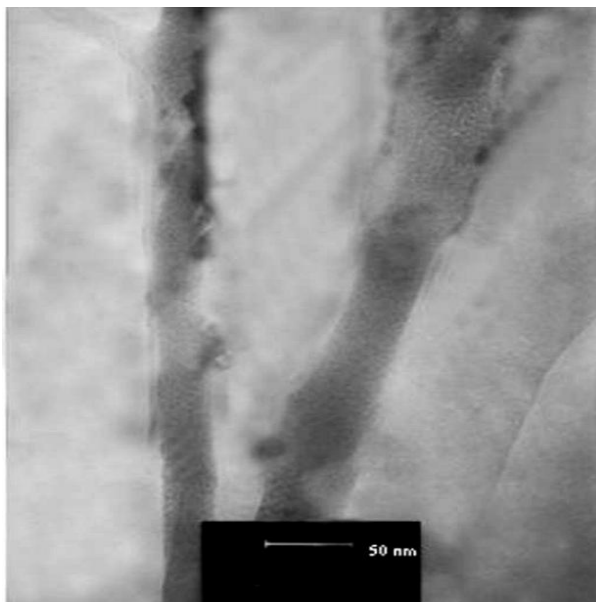


**Figure 8.** SEM images of the synthesized samples with different concentrations of SDS at 0.25% (a), 0.5% (b), 1% (c).

In a concentration of 0.5% wt, SDS molecules form cylindrical micelles with sulfate heads on the inside and outside surfaces that can form a complex compound with  $\text{Pb}^{2+}$ . These micellar structures control the rate of PbS formation.

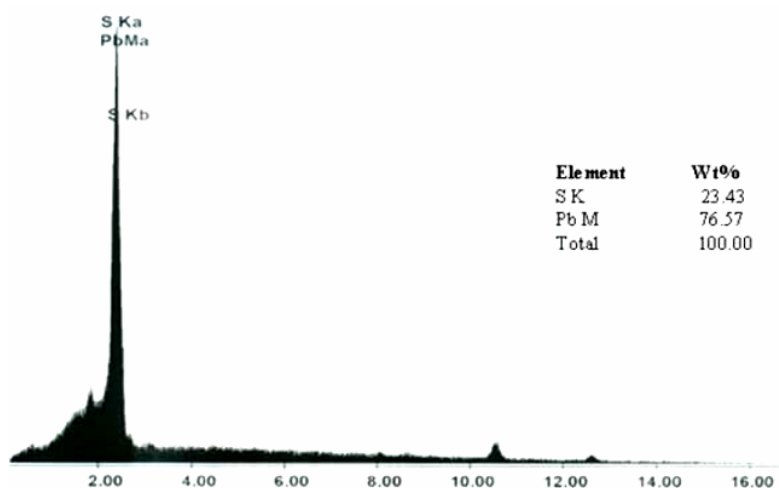
To recognize structure and properties of the synthesized sample in optimized conditions, it was characterized by TEM, Energy Dispersive X-ray (EDX), Uv-Vis spectroscopy, and TG/DT analyzers.

Figure 9 indicates the TEM image of the PbS nanowires under a magnification of 60000. Based on the TEM and SEM image in the optimum conditions, uniform PbS nanowires with 40-nm average diameter and 5- $\mu$  average length were synthesized.



**Figure 9.** TEM image of the optimized PbS nanowires with 60000 magnification.

The EDX patterns of the sample (Fig. 10) prove that the sample comprises only sulfur and lead elements without impurities.



**Figure 10.** EDX patterns for PbS sample which synthesized at 0.5% lead acetate, 1% sodium sulfide, 0.5 % SDS, pH 3, 2230W pulse power, and 25 °C solution temperature.

To study the effects of nanostructure morphology on the absorption spectrum, four various PbS samples were synthesized in different conditions according to Table 2.

Figure 11 illustrates SEM images of these samples. To investigate the absorption spectra of the cited samples, we dispersed 0.02 g of each sample in 10 ml of acetone. The absorption spectrum of the homogenized suspension was then recorded in the range of 300-400 nm. Figure 12 shows the Uv-Vis spectra of these samples.

**Table 2.** Experimental conditions for synthesizing of different PbS nanoparticles

Sample	Lead acetate concentration (% wt)	Sodium sulfide concentration (% wt)	pH	Solution temperature (°C)	Ultrasonic power (W cm <sup>-2</sup> )	SDS concentration (% wt)
1	0.5	1	3	25	2230	0.5
2	0.5	1	3	25	2230	0
3	0.5	1	3	25	-	0
4	0.5	1	Natural	25	-	0

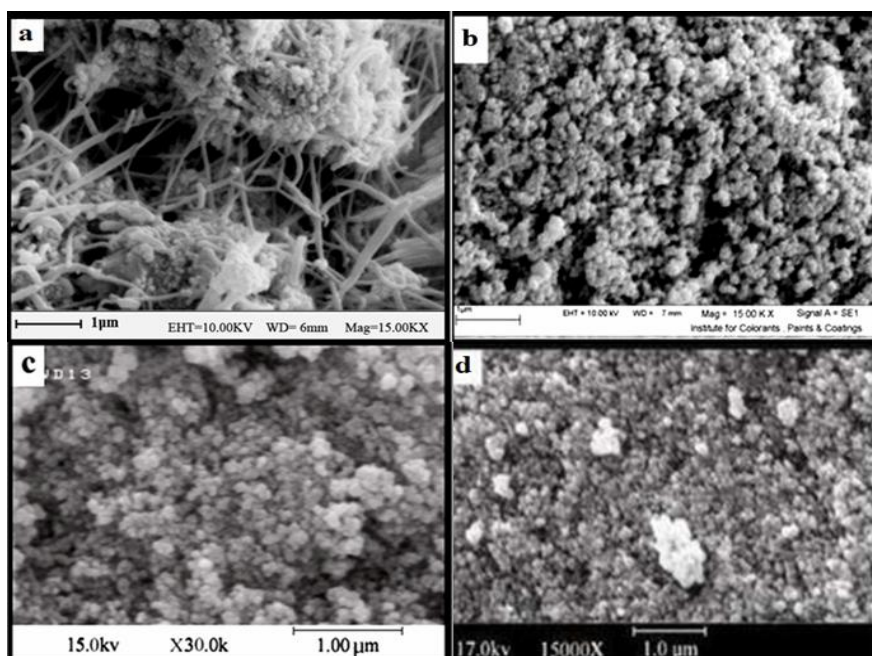


**Figure 11.** SEM images of the four synthesized samples in different conditions according to Table 2.

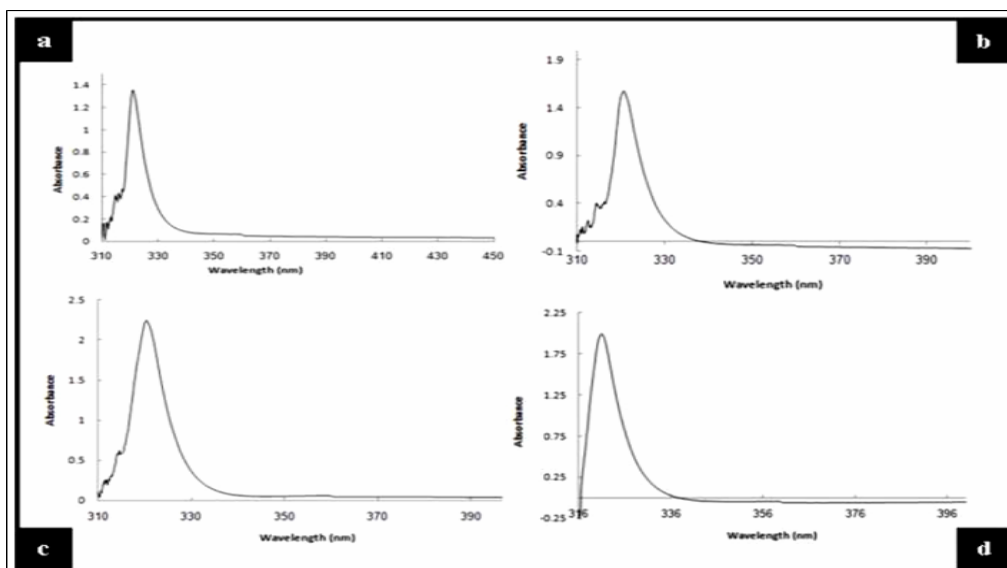


**Figure 12.** Uv-Vis spectra of the four synthesized samples in different conditions noted in Table 2; (a) sample 1, (b) sample 2, (c) sample 3, and (d) sample 4.

An energy gap of the samples was calculated by

$$(Eq. 2) \quad E = \frac{hc}{\lambda}$$

In Eq. 2, E (eV) is the energy gap, h ( $6.63 \times 10^{-34}$  J.s) is the Planck's constant, c ( $3 \times 10^8$  m.s<sup>-1</sup>) is the light velocity, and  $\lambda$  (nm) is the wavelength. The calculated data were summarized in Table 3.

**Table 3.** Absorbent wavelength and energy gap for different samples of PbS

Sample number according to Table 2	$\lambda_{max}$	Morphology	Particle size (nm)	Energy gap (eV)
1	321	Nanowire	38 (diameter)	3.872
2	320.8	Spherical nanoparticles	32	3.875
3	320.4	Spherical nanoparticles	90	3.879
4	321	Spherical nanoparticles	40	3.871

As seen in Table 3, the absorption wavelength value and energy gap of the samples are close to each other. In semiconductors with the energy gap being decreased, electrical conductance of the sample increases. Comparison between the energy gaps of the samples in Table 3 with previous references [4, 5] shows that the synthesized nanostructures have a wider energy gap (10 times more than previous reports). In the 3<sup>rd</sup> sample, the average particle size is 90 nm, which is larger than the other samples, and also the sample's energy gap (E) is longer than the other three samples. Consequently, an increase in the particle size causes a rise in the required energy to transmit the conducting electrons.

In the final stage, the synthesized PbS sample properties in optimum conditions were characterized by TGA and DTA. Figure 13 indicates TGA and DTA diagrams of PbS nanowires.

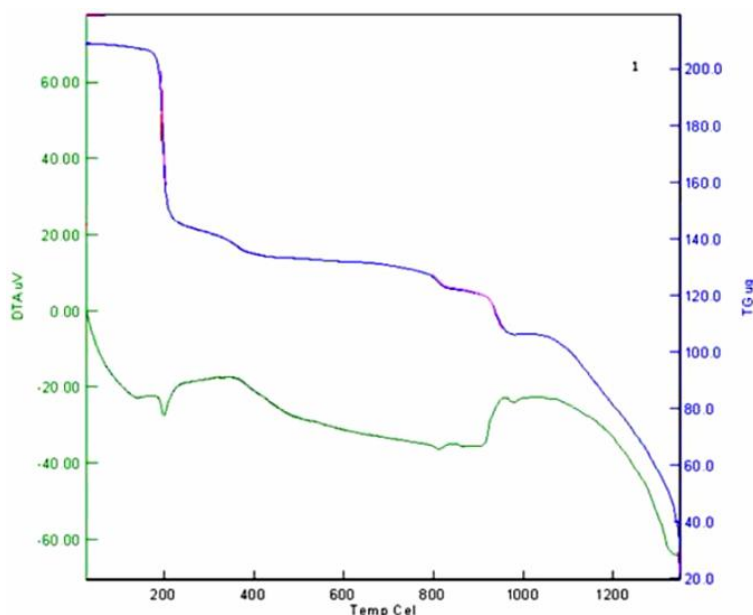


**Figure 13.** TGA and DTA curves of the synthesized sample in the optimum conditions.

The results of the DTA spectrum reveals that for the PbS sample, the peak descends at 200 °C; that implies to endothermicity and transformation of PbS to PbO. Also at a temperature of 950 °C,  $\alpha$ -type PbO changes to  $\beta$ -type and peak depression afterward are related to transformation of the solid lead to the melted one.

### 3.7. Application of PbS nanoparticles as a gas sensor

After optimization of the synthesized PbS sample, it was used as a gas-sensing agent. As mentioned in the experimental sections, the preparation steps were exactly performed. The effects of different gases like air, N<sub>2</sub>, CO, CO<sub>2</sub>, NO, NO<sub>2</sub>, SO<sub>2</sub>, and NH<sub>3</sub> were investigated on the Ohmic resistance of the prepared microchip (Fig. 14). As we can see in Fig. 14, a variation in the concentration of N<sub>2</sub>, air, CO, CO<sub>2</sub>, NO, and SO<sub>2</sub> doesn't considerably change the sensor's electrical resistance. Consequently, this sensor is unsuitable for measuring these gases, while the sensor shows good response to NH<sub>3</sub> and NO<sub>2</sub>.

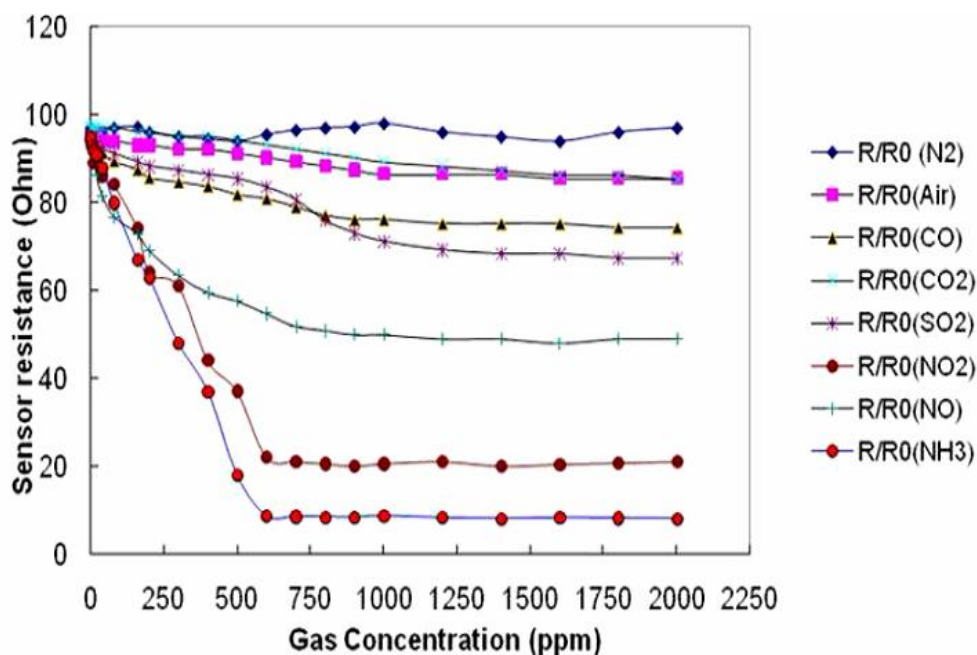


**Figure 14.** The sensor response for the different concentrations of various gases.

The calibration curves for the determination of NH<sub>3</sub> and NO<sub>2</sub> were shown in Figs. 15 and 16. As we can see in these figures, the sensor has linear range of 1 to 600 ppm for both NH<sub>3</sub> and NO<sub>2</sub> concentrations. The analytical sensitivity (the slope of calibration line) of the sensor is -0.115 and -0.145 ( $\Omega \text{ ppm}^{-1}$ ) for NH<sub>3</sub> and NO<sub>2</sub>, respectively. The sensitivity of the procedure to NH<sub>3</sub> is only 26% better than that to NO<sub>2</sub>. Therefore ammonia gas cannot be determined exactly in the presence of NO<sub>2</sub>. We tried to decrease the electrode sensitivity to NO<sub>2</sub> gas.

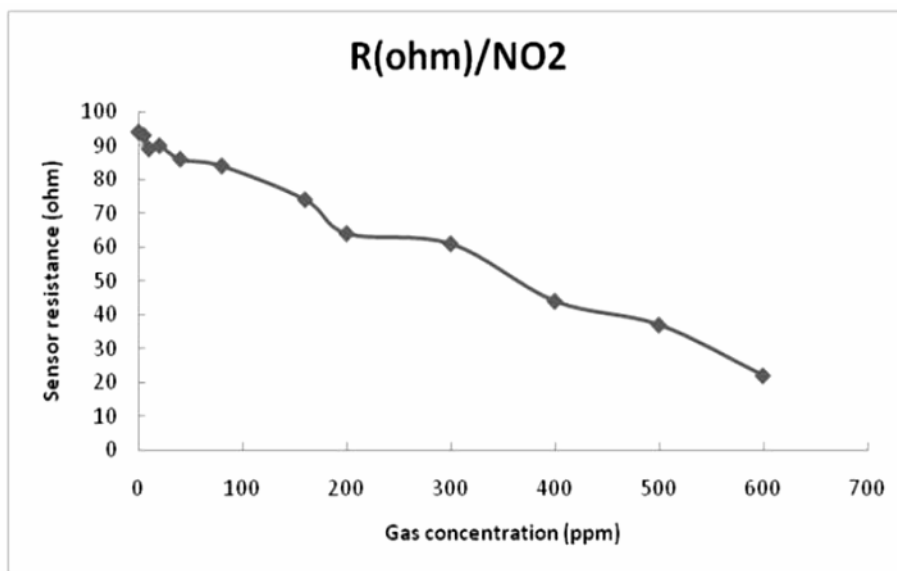


Figure 15. Calibration curve for measurement of NO<sub>2</sub>.

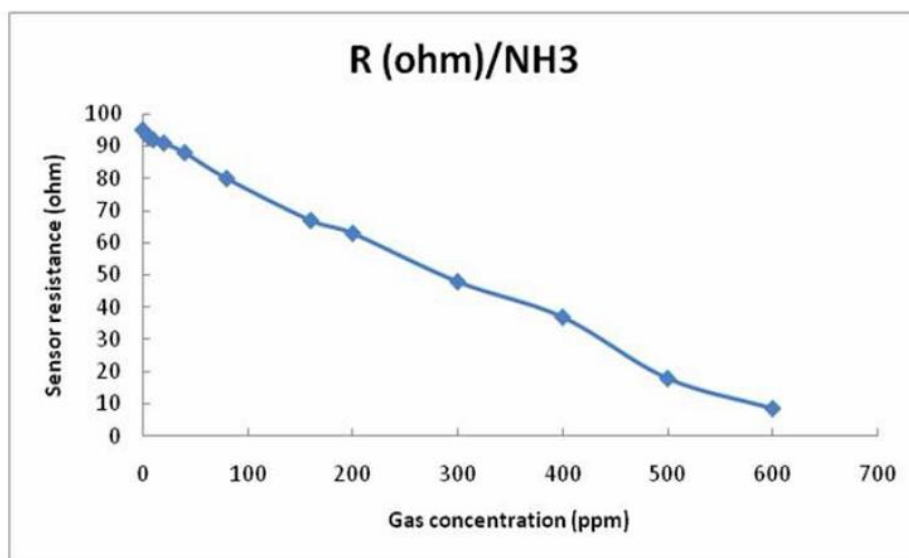


Figure 16. Calibration curve for measurement of NH<sub>3</sub>.

### 3.8. Modification of the sensor

With regard to reference [32], it is possible to increase sensor response to NH<sub>3</sub> in the presence of NO<sub>2</sub>. For this purpose, according to the mentioned method, about pure PbS, 2% wt ammonium chloride was added to PbS nanopowder, and the mixed powder was used as a gas-sensing agent and applied as a previous section to construct the ammonia gas sensor.

Figure 17 shows the modified sensor response to the NH<sub>3</sub> and NO<sub>2</sub> gases. As we can see in this figure, when ammonium chloride is used as a sensor modifier, the electrode response to the NO<sub>2</sub> gas is greatly decreased. The calibration equations for NO<sub>2</sub> and NH<sub>3</sub> were calculated as  $(y = -0.152 x + 92.62)$

and ( $y = -0.048 x + 93.94$ ), respectively. The obtained results showed that the presence of ammonium chloride causes the electrode response to the  $\text{NO}_2$  gas to decrease about 58%. After using the added ammonium chloride, the sensor sensitivity to  $\text{NO}_2$  was 69% lower than its response to  $\text{NH}_3$ . In the modified state, the electrode can be successfully used for the determination of  $\text{NH}_3$  in the presence of  $\text{NO}_2$ .

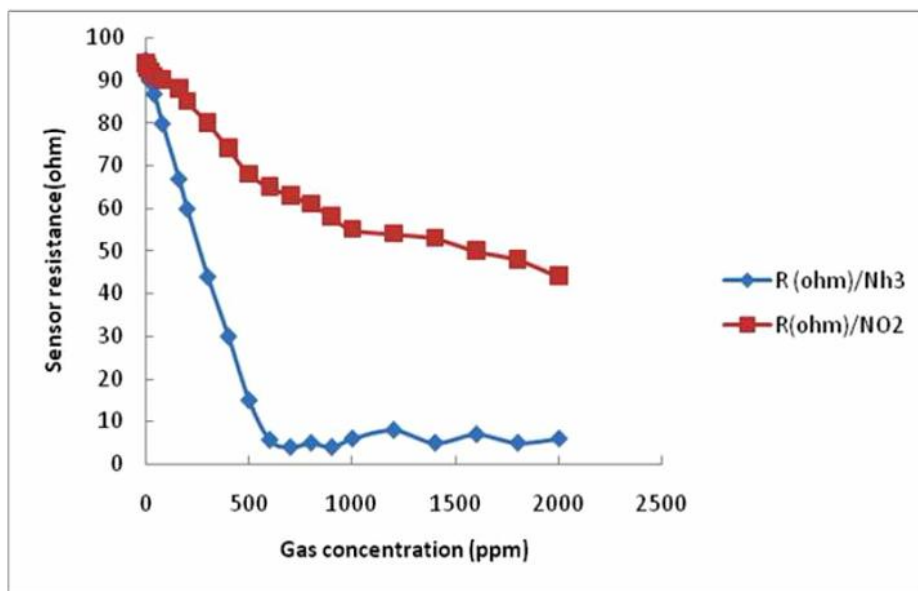


Figure 17. The response curves the modified sensor for  $\text{NH}_3$  and  $\text{NO}_2$  gases.

### 3.9. Sensor ability for the measurement of $\text{NH}_3$

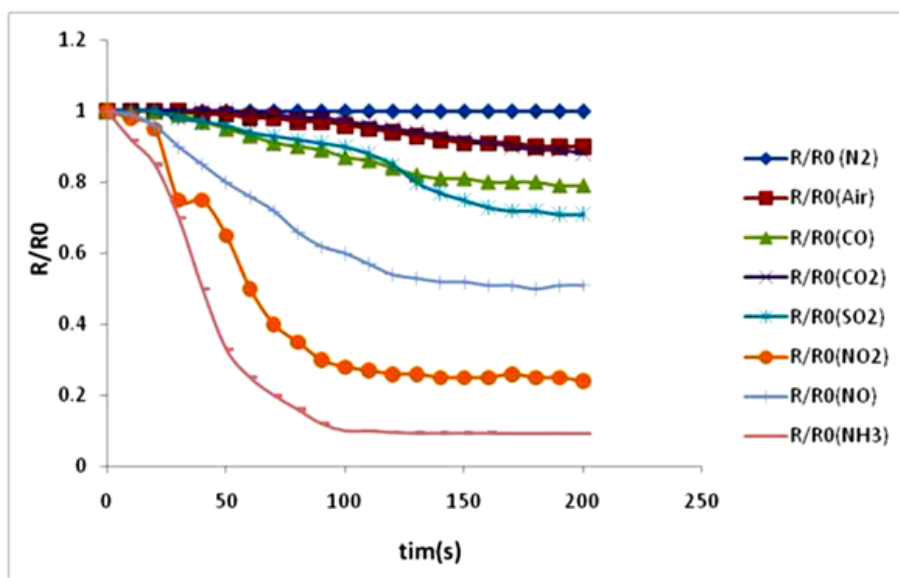
The modified sensor was applied to measure the concentration of  $\text{NH}_3$  in an artificial medium with 120 ppm  $\text{NH}_3$ , 240 ppm  $\text{NO}_2$ , and in air with 360 ppm  $\text{NO}$ , 360 ppm  $\text{CO}$ , and 360 ppm  $\text{CO}_2$ . The results are presented in Table 4. The precision of the results was confirmed by T-test. The value of  $t_{n-1}$  with a confidence level of 95% is equal to 3.18. The experimental  $t$  (0.12) is less than 3.18; consequently, the average value of four measurements (119.75 ppm) lack significant difference from the real value (120 ppm).

Table 4. The found values for 120 ppm  $\text{NH}_3$  in a sample including  $\text{CO}$  (360 ppm),  $\text{CO}_2$  (360 ppm),  $\text{NO}$  (360 ppm), and  $\text{NO}_2$  (240 ppm)

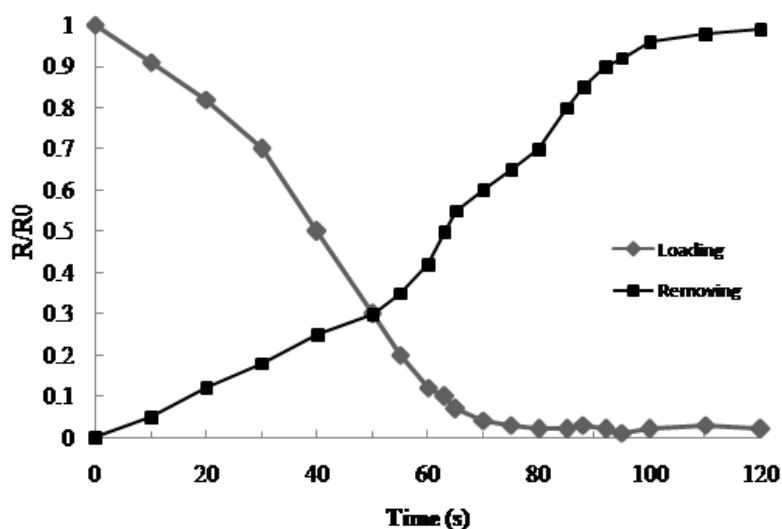
Repetition	Measured concentration of $\text{NH}_3$ (ppm)
1	124
2	122
3	118
4	115

3.9. Sensor response time

To obtain response time, we determined the changes in relative sensor resistance versus the time. Figure 18 shows the changes in sensor relative resistance for different gases like N<sub>2</sub>, Air, CO, CO<sub>2</sub>, NO, SO<sub>2</sub>, NO<sub>2</sub>, and NH<sub>3</sub> during 200 s. As we see in Fig. 18, the sensor- relative resistance for N<sub>2</sub>, Air, CO, CO<sub>2</sub>, and SO<sub>2</sub> doesn't clearly change with time, but for NO, NO<sub>2</sub>, and NH<sub>3</sub>, it does decrease over time. Table 5 presents the comparison of the response times of NO, NO<sub>2</sub>, and NH<sub>3</sub>. It is obvious that the response time for NH<sub>3</sub> is shorter than those of NO and NO<sub>2</sub>. Therefore the constructed sensor can be used to measure NH<sub>3</sub> dosage in the presence of the other interfering gases.



(a)



(b)

Figure 18. Time dependence of the sensor response for 120 ppm different gases.

**Table 5.** The sensor response time for NH<sub>3</sub>, NO, and NO<sub>2</sub> gases at concentrations of 120 ppm

Gas	Response time (s)
NH <sub>3</sub>	60
NO <sub>2</sub>	75
NO	111

#### 4. CONCLUSIONS

PbS nanowires can be prepared by using rate control adding lead acetate solution to a sodium sulfide solution. In this method, sodium sulfide and lead acetate concentration, type and concentration of synthesis additive, pH, bath temperature, and ultrasonic wave radiation are effective parameters that can change the morphology and the particle sizes of a sample. SDS can be used as a suitable additive to control the morphology of PbS nanowires. The PbS nanowires act as successive and sensitive agents in the solid-state sensor to measure ammonia concentration in the gas mixtures.

#### ACKNOWLEDGEMENT

We gratefully acknowledge the support of this work by Abhar Payame Noor University Research Council.

#### References

1. J. Zhu, S. Liu, O. Palchaik, Y. Kolytyn, A. Gedanken, *J. Solid State Chem.* 153 (2000) 342-348.
2. F. E. Kruis, H. Fissan, B. Rellinhaus, *Mater. Sci. Eng. B* 69–70 (2000) 329-334.
3. F.E. Kruis, H. Fissan, A. Peled, *J. Aerosol Sci.* 29 (1998) 511-535.
4. J. L. Machol, F. Wise, R. C. Patel, D. B. Tanner, *Phys. Rev. B* 48 (1993) 2819-2822.
5. S. Zhou, Y. Feng, *J. Mater. Res.* 18 (2003) 1188-1193.
6. G. Ujjal K, S. Ram. *Mater. Res. Bull.* 39 (2004) 669-676.
7. Wang SF, Gu F, Lu MK, Zhou GJ, Zhang AY. *J. Cryst. Growth* 289 (2006) 621-625.
8. T. Saraidarov, R. Reisfeld, A. Sashchiuk, E. Lifshitz. *Physica E*. 37 (2007) 173-177.
9. Z. Wanqun, Y. Qing, X. Liqiang, Y. Weichao, Q. Yitai. *Mater. Lett.* 59 (2005) 3383-3388.
10. Z. Guangjun, L. Mengkai, X. Zhiliang, W. Shufen, Z. Haiping, Z. Yuanyuan, and W. Shumei. *J. Phys. Chem. B* 110 (2006) 6543-6548.
11. Z. Zhihua, L. Sie Huey, V. Jagadese J, C. Wee Shong. *J. Phys. Chem. B* 110 (2006) 6649-6654.
12. N. Yonghong, F. Wang, L. Hongjiang, Y. Gui, H. Jianming, M. Xiang, X. Zheng. *J. Cryst. Growth* 262 (2004) 399-402.
13. W. Shiquan, P. Anlian, Y. Haoyong, H. Yuping, L. Yun, X. Zhude, Z. Bingsuo. *Mater. Lett.* 60 (2006) 1242-1246.
14. N.I. Fainer, M.L. Kosinova, Yu.M. Romyantsev, E.G. Salman, F.A. Kuznetsov, *Thin Solid Films* 280 (1996) 16-19.
15. A. Mondal, N. Mukherjee, *Mater. Lett.* 60 (2006) 2672-2674.
16. J. Vaitkus, V. Kazlauskienė, J. Miskinis, J. Sinius, *Mater. Res. Bull.* 33 (1998) 711-716.
17. B. Thangaraju, P. Kaliannan, *Semicond. Sci. Technol.* 15 (2000) 849-853.

18. R. Resch, G. Friedbacher, M. Grasserbauer, T. Kannianen, S. Lindoors, M. Leskela, L. Nijnisto. *Appl. Surf. Sci.* 120 (1997) 51-57.
19. M. Ichimiura, T. Narita, K. Masui. *Mater. Sci. Eng. B* 96 (2002) 296-299.
20. A. P. Gaiduk, P. I. Gaiduk, A. N. Larsen. *Thin Solid Films*. 516 (2008) 3791-3795.
21. X. Changqi, Zh. Zhicheng, W. Hailong, Y. Qiang. *Mater. Sci. Eng. B* 104 (2003) 5-8.
22. V. F. Markov and L. N. Maskaeva, *J. Anal. Chem.* 56 (2001) 754-757.
23. S. Bandyopadhyay, *Part. Sci. Tech.* 30 (2012) 43-54.
24. Y. Hu, Z. Zhang and C. Yang, *Ultrasonic Sonochem.* 15 (2008) 665.
25. D. Bremner, A. E. Burgess and F. B. Li, *Appl. Catalysis*, 203 (2000) 111.
26. A. Phuruangrat, T. Thongtem, and S. Thongtem, *Mater. Lett.* 63 (2009) 667-669.
27. A. Phuruangrat, T. Thongtem, S. Thongtem, *Appl. Surf. Sci.* 254 (2008) 7553-7558.
28. G. Lelong, S. Bhattacharyya, S. Kline, T. Caccia guerra, M. A. Gonzalez, M. L. Saboungi, *J. Phys. Chem. C* 112 (2008) 10674-10680.
29. J. Lee, T. Isob, M. Senna, *Colloid Interface Sci.* 177 (1996) 490-494.
30. C. W. Kwon, T.S Yoon, S. S. Yim, S. H. Park and K. B. Kim, *J. Nanopart. Res.* 11 (2009) 831-839.
31. Z. Y. Yuan, T. Re and B. L. Su, *J. Catalysis Today* 95 (2004) 743-750.
32. T. Fu, *Sens. Actuators B* 140 (2009) 116-121.